Article

A Mimic Peroxidase- and Bi2S3 Nanorod-Based Photoelectrochemical Biosensor for Signal-On Detection of Polynucleotide Kinase

Lin Cui, Juan Hu, Meng Wang, Xing-kang Diao, Chen-chen Li, and Chun-yang Zhang

Anal. Chem., **Just Accepted Manuscript** • DOI: 10.1021/acs.analchem.8b02673 • Publication Date (Web): 29 Aug 2018

A Mimic Peroxidase- and Bi_2S_3 Nanorod-Based Photoelectrochemical Biosensor for Signal-On Detection of Polynucleotide Kinase

Lin Cui,[†] Juan Hu,[†] Meng Wang,[†] Xing-kang Diao, Chen-chen Li, and Chun-yang Zhang*

College of Chemistry, Chemical Engineering and Materials Science, Collaborative Innovation Center of Functionalized Probes for Chemical Imaging in Universities of Shandong, Key Laboratory of Molecular and Nano Probes, Ministry of Education, Shandong Provincial Key Laboratory of Clean Production of Fine Chemicals, Shandong Normal University, Jinan 250014, China.

* Corresponding author. Tel.: +86 0531-86186033; Fax: +86 0531-82615258. E-mail: cyzhang@sdnu.edu.cn.

ABSTRACT: We demonstrate for the first time the development of a mimic peroxidase- and bismuth sulfide (Bi_2S_3) nanorod-based photoelectrochemical (PEC) biosensor for signal-on detection of polynucleotide kinase (PNK) on the basis of manganese-based mimic enzyme (MnME) catalytic precipitation. We use the hybrid film which consists of Bi_2S_3 nanorods and Au nanoparticles (AuNPs) as the immobilization matrix of capture probe. The capture probe on the modified electrode can specifically hybridize with the MnME@AuNPs-labeled signal probe to form the double-stranded DNA (dsDNA), generating a PEC biosensor. In the absence of PNK, MnME may stimulate the mimic enzyme catalytic precipitation onto the electrode surface, blocking the interfacial electron transfer and eventually leading to a low PEC signal. While in the presence of PNK, the dsDNA is phosphorylated and subsequently cleaved by lambda exonuclease to release the MnME@AuNPs conjugates from the electrode, leading to the decrease of catalytic precipitation on the surface of electrode and consequently the production of a high PEC signal. Notably, the MnME can be easily synthesized and possesses higher catalytic activity than the manganese-based mimic enzyme. This signal-on PEC biosensor exhibits high sensitivity with a detection limit of 1.27×10^{-5} U mL^{-1} and an extrembly large dynamic range of 5 orders of magnitude. Moreover, it can be applied for the screening of PNK inhibitors and accurate quantification of PNK activity in cancer cell extracts.

INTRODUCTION

Photoelectrochemical (PEC) biosensor is a promising analytical method with distinct advantages of simple instrument, high sensitivity, and easy miniaturization,[1] and it has been widely applied for enzyme assay, nucleic acids analysis, and the detection of small biomolecules.[2-5] To improve the capacity of converting photoirradiation to electrical signal, a series of photocatalyst such as TiO_2 and ZnO have been introduced in the development of PEC biosensors. Despite their high photo-to-current conversion efficiency, the application of TiO_2 and ZnO in PEC biosensing is limited by following factors: (1) the wide band gap (3.2 eV for TiO_2[6] and 3.44 eV for ZnO[7]) does not benefit the generation of PEC signal under visible light, (2) they mainly absorb UV light with high energy, which may damage organic analytes and biomolecules. To overcome these issues, a variety of semiconducting materials with high catalytic activity under visible-light irradiation have been introduced, including CdS,[8] CdSe,[9] graphite-like carbon nitride (g-C_3N_4),[10] Ag_2S,[11] and PbS.[12] However, the cadmium contamination and photocorrosion prevent their practical applications. Bismuth sulfide (Bi_2S_3) is an important type of semiconductors that exhibits a broad absorption overlapping with the near-IR and visible spectra as well as the tunable band gap. Moreover, Bi_2S_3 may function as the light-harvesting substrate for the development of PEC biosensors due to its high incident-photon-to-electron-conversion efficiency and high absorption coefficient.[13,14] A variety of Bi_2S_3 (e.g., Bi_2S_3 nanotube and nanoparticle thin film,[13] Bi_2S_3 nanorods,[14] Bi_2S_3 nanoflake,[15] Bi_2S_3 nanosheet,[16] Bi_2S_3@MoS_2 nanoflowers[17]) may function as the photoactive materials of PEC sensors for the detection of methylated DNA,[14] microRNA,[17] DNA methyltransferase,[15] avian leucosis virus,[18] and sulfadimethoxine.[19]

To amplify the response signal and improve the sensitivity, several enzyme-mediated signal amplification-based PEC sensors have been designed with the advantages of simplicity, low-cost construction, high biocatalytic activities and good specificity.[20-22] The easiest way is the use of enzyme reaction to produce an insoluble product on the transducer, which may generate a physical effect (e.g., steric hindrance and insulating effect) to block the interfacial electron communication between the PEC species and the electron acceptor/electron donor substances.[23] However, most of the PEC detection strategy is signal-off assay due to the involvement of enzyme reaction to produce an insoluble product.[23-25] The signal-off sensor suffers from the false positivity and the limited signal gain because the target can only suppress 100% original current.[26-28] To achieve signal

amplification, the natural enzymes such as horseradish peroxidase (HRP) are introduced to catalyze the formation of particular products (e.g., insoluble benzo-4-chlorohexadienone from HRP accelerated oxidation).[23-25] Nevertheless, the stability of natural enzymes is relatively poor due to their easy denaturation by environmental changes, and the preparation, purification and storage of natural enzymes are usually time-consuming and expensive.[29] Alternatively, some artificial enzyme mimetics (nonenzymatic enzyme-mimicking) such as carbon materials,[30] metal nanoparticles,[31] metal oxides,[32] and hemin[33,34] have been developed with good stability and high catalytic activity. Especially, the enzyme mimetics based on metal nanostructures with silver iodide-chitosan nanoparticles,[35] Pt nanoparticles,[36] and PtCu nanoframes[37] as the peroxidase mimics have distinct advantages of controllable synthesis, high catalytic activity, and good stability against stringent conditions. Thus, the integration of novel enzyme mimic may provide new approach for the development of new PEC sensing strategy.

In this research, we develop a signal-on PEC biosensor for signal amplified detection of PNK based on the manganese-based mimic enzyme (MnME) catalytic precipitation with Bi_2S_3 nanorods as the PEC species. The PEC biosensor has significant advantages: (1) in contrast to the reported signal-off biosensors,[38,39] this biosensor generates a signal-on PEC signal; (2) the Bi_2S_3 nanorods as the photoactive materials can be excited by visible light for the generation of a high photocurrent; (3) the MnME catalytic precipitation not only leads to the formation of an insulating barrier, but also enhances the steric hindrances, efficiently excluding the false-positive signal; (4) the MnME is easily synthesized and functionalized with the biomolecules; (5) the MnME possesses a higher catalytic activity than the manganese-based mimic enzymes, greatly improving the detection sensitivity. We demonstrate the application of this signal-on PEC biosensor for accurate quantification of PNK activity and the screening of potential PNK inhibitors.

EXPERIMENTAL SECTION

Reagents and Material. Chloroauric acid ($HAuCl_4 \cdot 4H_2O$) and trisodium citrate were obtained from Shanghai Reagent Company (Shanghai, China). Bismuth nitrate ($Bi(NO_3)_3$), sodium sulfide (Na_2S), ascorbic acid (AA), o-diaminobenzene (OPD), glycoland urea were purchased from Aladdin (Shanghai, China). Horseradish peroxidase (HRP), adenosine diphosphate (ADP), lysozyme, bovine serum albumin (BSA), adenosine triphosphate (ATP), tris(hydroxymethyl)aminomethane(tris), tris-(2-carboxyethyl) phosphine hydrochloride

(TCEP), and mercaptohexanol (MCH) were purchased from Sigma-Aldrich Chemical Co. (St. Louis, MO, USA). The protein kinase A (PKA), E. coli ligase, T4 DNA ligase, lambda exonuclease (5 U μL^{-1}), and T4 polynucleotide kinase (10 U μL^{-1}) were obtained from New England Biolabs (NEB, UK). The 3,3-diaminobenzidine (DAB) was bought from Sinopharm Chemical Reagent Co., Ltd. (Beijing, China). Hydrogen peroxide (H_2O_2, 30%) was obtained from Changsha Antai Chemical Industry Co. Ltd. (Changsha, China). The indium tin oxide (ITO) electrode was purchased from Zhuhai Kaivo Electronic Components Co. Ltd. (Zhuhai, China). Acetate buffer solutions (HAc-NaAc, pH 5) were prepared by mixing the stock solutions of 0.1 M sodium acetate (CH_3COONa) and 0.1 M acetic acid (CH_3COOH). All the other chemicals with analytical grade were used without further purification. The ultrapure water from a Millipore water purification system (≥18 MΩ, Milli-Q, Millipore) was used to prepare the aqueous solutions. All the oligonucleotides (**Table 1)** were obtained from Takara Biotech. Co. Ltd. (Dalian, China).

Table 1. Sequences of the Oligonucleotides

name	sequence (from 5' to 3')
capture probe (P1)	OH-CGA CTC AGA CAC ATG-$(CH_2)_6$-SH
signal probe (P2)	OH-CAT GTG TCT GAG TCG TTT TT-$(CH_2)_6$-SH

The binding regions in probe 1 and probe 2 were shown in underlined.

Apparatus and Characterization. The photoelectrochemical detection was performed on a Zahner workstation (Zahner, German) by using a light (700 W/m^2, λ = 470 nm) as the light source at a constant potential of 0 V. All electrochemical and photoelectrochemical experiments were performed with a modified ITO electrode (4 mm in diameter) as the working electrode, a saturated calomel as the reference electrode, and a platinum electrode as the auxiliary electrode at room temperature. Electrochemical impedance spectroscopy (EIS) was measured in 5 mM $[Fe(CN)_6]^{3-/4-}$ redox couple solution (1:1 molar ratio) containing 0.1 M KCl in the frequency range of 10 kHz - 0.1 Hz. Scanning electron microscopic (SEM) images were collected on a Sirion-100 (FEI) and a SU-8010 (Hitachi) scanning electronic microscope. Powder X-ray diffraction (XRD)

patterns were obtained by a Rigaku D/MAX 2200PC X-ray diffractometer (Japan) with Cu Kα radiation (λ = 0.154178 nm, graphite monochromator, 28 kV and 20 mA), a 2θ range from 10° to 80° at a scanning speed of 10° min^{-1}. Zeta potential was measured with a Malvern Zeta Sizer Nano (Malvern Instruments). The transmission electron micrographs (TEM) were obtained by a JEOL JEM 2010 electron microscope at 200 kV. Atomic force microscope (AFM) imaging was performed on a Cypher VRS AFM (Oxford Instruments) in tapping mode by using an AC240TS probe in a scan rate of 2.44 Hz.

Synthesis of MnME and MnME@AuNPs-P2. MnME nanocubes were synthesized via a simple chemical precipitation method according to the previous report with some modifications.[40] Briefly, 2 mg of chitosan was dissolved in a solution containing 10 mL of C_2H_5OH, 10 mL of H_2O and 1% acetic acid; and then 0.045 g of $MnSO_4 \cdot H_2O$ was added into the above solution. At the same time, 0.066 g of $K_3Fe(CN)_6$ was dissolved in 10 mL of ultrapure water. These two solutions were mixed and stirred violently for 60 min at room temperature, and then the resultant black-gray mixture was filtered and washed several times with absolute ethanol and dried at room temperature. The MnME was further modified with AuNPs by mixing 4 mL of AuNPs (13 nm diameter) solution[41] with 2 mL of chitosan-modified MnME (2 mg mL^{-1}) and shaking vigorously for 2 h. The obtained MnME@AuNPs composite was collected by centrifugation, washed with ultrapure water for three times, and dispersed in 2 mL of 50 mM Tris-HCl buffer (pH 7.4). After the P2 was activated with 5 μL of 10 mM TCEP to reduce disulfide bond, it was mixed with 500 μL of MnME@AuNPs suspension, followed by incubation at room temperature for 24 h to obtain MnME@AuNPs-P2. Then the MnME@AuNPs-P2 was blocked with 1% BSA (w/v) for 1 h and dispersed in 500 μL of 50 mM Tris-HCl buffer (containing 300 mM NaCl, pH 7.4) to store at 4 °C before use. The surface charges of the MnME, MnME@AuNPs and the MnME@AuNPs-P2 were compared by monitoring the changes in zeta-potential.

Synthesis of Bi_2S_3 Nanorods. The Bi_2S_3 nanorods was synthesized according to the previous report with some modifications.[42] In brief, 1.82 g of $Bi(NO_3)_3 \cdot 5H_2O$ was added into 25 mL of ethanediol and stirred for 20 min. Meanwhile, 1.35 g of $Na_2S \cdot 9H_2O$ was added into 30 mL of ultrapure water and stirred for 1 h. The 1.92 g of carbamide was added into 20 mL of ultrapure water. Then $Na_2S \cdot 9H_2O$ solution was added into $Bi(NO_3)_3 \cdot 5H_2O$ solution drop by drop. A large number of black suspension materials were produced in the mixed solution. Subsequently, carbamide solution was poured into the above solution, and then transferred to a Teflon-lined stainless-steel autoclave (100-mL capacity), sealed and maintained at 180 ^oC for 24 h. The

resultant black solid product was filtered, washed with ultrapure water and ethanol, and finally dried in air.

Fabrication of Photoelectrochemical Biosensor. The ITO slices were cut into 4.7 cm × 1 cm pieces, sonicated in 1.0 M NaOH, 10% H_2O_2, and acetone, followed by cleaning with ultrapure water thoroughly and blow-drying with nitrogen prior to use. Then 10 μL of 2 mg mL^{-1} Bi_2S_3 and AuNPs solution were sequentially dropped on the working electrode. After drying at room temperature, the Bi_2S_3 and AuNP-modified electrode was washed with ultrapure water and dried with nitrogen. Meantime, the thiolated P1 (0.1 μM) was activated by 10 μM TCEP for 1 h to reduce the disulfide bonded oligos. Then 10 μL of P1 was pipetted onto the above modified working electrode and incubated overnight at room temperature in 100% humidity. After rinsing with 50 mM Tris-HCl buffer (pH 7.4), the working electrode was passivated with 1 mM MCH for 2 h to block the nonspecific adsorption sites. Then the electrode was rinsed with 10 mM Tris-HCl buffer (pH 7.4) and dried in nitrogen, followed by incubation with the MnME@AuNPs-P2 conjugates in 10 mM Tris-HCl buffer (pH 7.4) containing 100 mM NaCl for 2 h at 37 ^oC. The electrode was stored at 4 °C after thoroughly rinsing and dring in nitrogen.

Photoelectrochemical Measurement of PNK Activity. After the incubation of the PEC biosensor with 10 μL of reaction solution containing different-concentration PNK and 1 mM ATP for 30 min at 37 °C and the rinsing of electrode for three times with 10 mM Tris-HCl buffer (pH 7.4), the 0.1 U μL^{-1} lambda exonuclease was added the surface of electrode and incubated for 50 min at 37 °C. Subsequently, 5 μL of 1.0 mg mL^{-1} DAB and 5 μL of 0.01 M H_2O_2 were added onto the electrode surface for 5 min to allow the occurrence of enzymatically catalyzed reaction. After rinsing with 10 mM Tris-HCl buffer (pH 7.4), the electrodes were subjected to PEC measurements.

Inhibition Assay. The $(NH_4)_2SO_4$, NaH_2PO_4 and ADP were selected as the PNK inhibitors. The different-concentration inhibitors were incubated with 1 U mL^{-1} PNK reaction buffer, followed by the similar experimental procedures for PNK assay described above.

Preparation of Cell Extracts. The human embryonic kidney cells (HEK293T cells) were cultured in Dulbecco's modified Eagle's medium (DMEM, Life Technologies, USA) with 10% fetal bovine serum (FBS, Life Technologies, USA) and 50 U mL^{-1} of penicillin plus 50 μg mL^{-1} streptomycin at 37 °C with 5% CO_2. To perform the real sample analysis, the cell extracts were prepared using a nucleoprotein extraction kit (BSP001, Sangon Biotech, Shanghai, China) according to the manufacturer's protocol.

RESULTS AND DISCUSSION

Design of PEC Biosensor. The principle of signal-on PEC biosensor is shown in Scheme 1. The sequences of capture probe (P1) and signal probe (P2) were designed to be partially complementary to each other, and they were modified with thiol at the 3' end. The P2 may be linked on the surface of MnME@AuNPs through Au-S covalent binding to form the MnME@AuNPs-P2 conjugates. The P1 is firstly immobilized on the Bi_2S_3- and AuNP-modified ITO electrode by layer-by-layer self-assembly via the Au-S bond. Notably, the P1 may serve as the capture probe to bind the MnME@AuNPs-P2 for the formation of MnME@AuNPs-P2/P1 structure, introducing MnME to the Bi_2S_3- and AuNP-modified ITO electrode surface. In the absence of PNK, no lambda exonuclease-mediated cleavage reaction occurs due to the lack of 5'-phosphoryl, and the MnME@AuNPs-P2 conjugates are maintained on the surface of electrode. The MnME exhibits excellent mimic peroxidase property and it can accelerate the oxidation of DAB by H_2O_2, generating insoluble and insulating product which deposits on the transducer surface (Scheme S1, see Supporting Information) to build up an insulating layer on the electrode. This insulating layer may hinder the diffusion and electron transfer of AA on the electrode/solution interface to donate electron for the photogenerated holes of Bi_2S_3. In addition, the steric hindrance of MnME may block the transfer of AA to electrode surface. As a result, the photocurrent of biosensor is inhibited, with a negligible photocurrent being observed. In the presence of PNK, it catalyzes the transfer of gama-phosphate residue from ATP to the 5'-hydroxyl end, generating the 5'-terminal phosphorylated P2-P1 dsDNA. The subsequent digestion of the phosphorylated P2-P1 dsDNA by lambda exonuclease induces the dissociation of the MnME@AuNPs-P2 conjugates from the surface of electrode and the reduction of the insoluble precipitation amount and consequently the increase of photoelectrochemical signal. The change in photoelectrochemical signal is proportional to the PNK concentration.

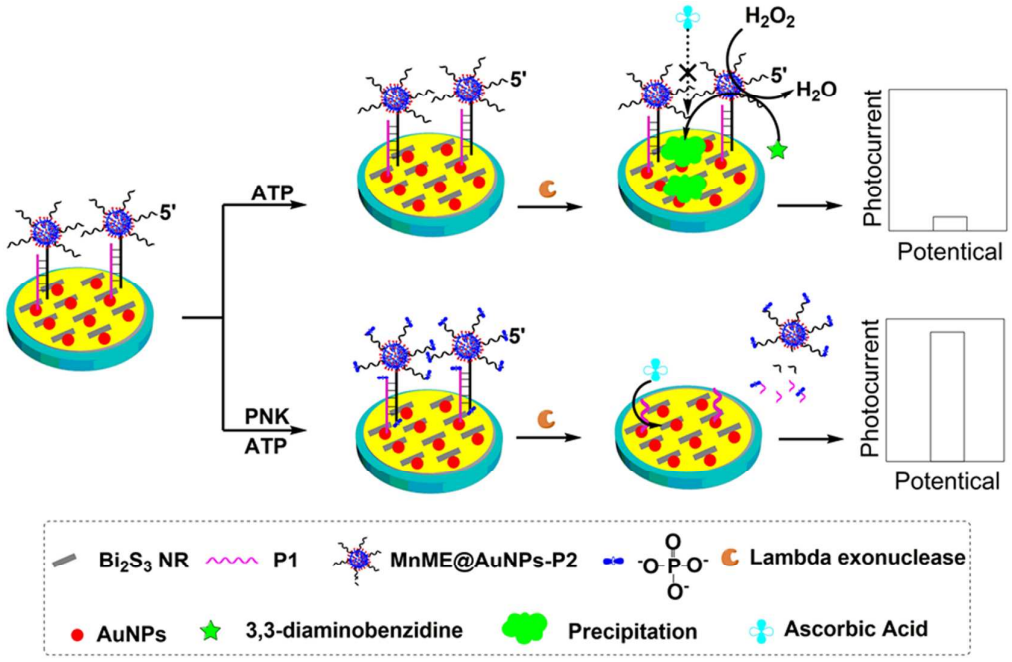

Scheme 1. Schematic Illustration of a Signal-on Photoelectrochemical Biosensor for PNK Assay with the MnME@AuNPs-P2 Catalytic Insoluble Precipitation on Bi_2S_3 Nanorod as the Photoactive Materials.

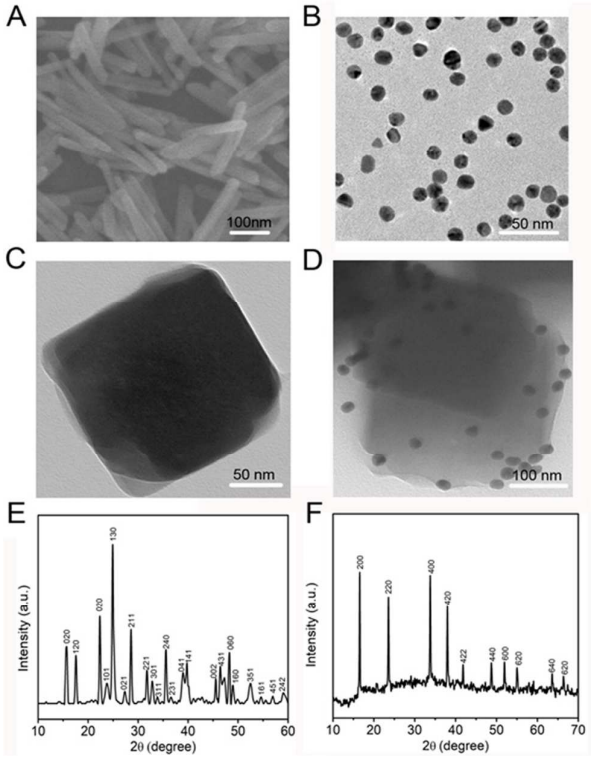

Figure 1. (A) SEM images of Bi_2S_3. (B-D) TEM images of AuNPs (B), MnME (C), MnME@AuNPs (D).

(E-F) XRD pattern of Bi_2S_3 (E) and MnME (F).

Characterization of Different Nanomaterials. The morphology and structure of Bi_2S_3 were investigated by SEM. As shown in Figure 1A, the Bi_2S_3 structure consists of large amounts of nanorods with 10-20 nm in diameter and 100-200 nm in length. As shown in Figure 1B, the average diameter of AuNPs was 13 nm. TEM images were taken to characterize the morphology of MnME (Figure 1C). The cubic structure of MnME is well-defined and uniform with a diameter of about 200 nm, and the surfaces of the cubes are extremely smooth. As shown in Figure 1D, the AuNPs were well dispersed on the surface of MnME matrix, confirming the successful modification of AuNPs on MnME. The zeta potential was used to investigate the linking of AuNPs to MnME. The zeta potential of MnME in PBS (pH 7.4) was determined to be 10.2 ± 0.4 mV, which allowed for its electrostatic interaction with the negatively charged citrate-capped AuNPs. The reversed zeta potential of -2.28 ± 0.5 mV indicated that AuNPs were successfully coated onto the MnME surface. When P2 was grafted onto the MnME@AuNPs-P2 via the Au-S bond between the thiol groups on P2 and AuNPs, a higher negative zeta potential (-4.5 ± 0.2 mV) was observed. The phase of Bi_2S_3 nanorods were further characterized by XRD (Figure 1E). The perfect match of the diffraction peaks of the powders with the Bi_2S_3 standard card (JCPDS: 17-0320) suggests the orthorhombic phase of pure Bi_2S_3.[18] The XRD pattern of MnME shows that all the reflections can be indexed to the pure face-centered cubic phase of $Mn_4Fe(CN)_{62.667}\cdot 15.84H_2O$ (ICSD-151693) (Figure 1F), with the sharp and strong peaks implying the high purity and good crystallinity of the product. In addition, the diffuse reflection spectrum of Bi_2S_3 nanorod was characterized (Figure S1, see Supporting Information).

The peroxidase-like catalytic performance of MnME was evaluated using a colorimetric oxidation reaction with DAB as the substrate[43] (Figure 2). The mixture of DAB and H_2O_2 remained clear and colorless (Figure 2a). Upon the addition of 1 μL of 1 mg mL^{-1} HRP suspension to 100 μL of the mixture of DAB and H_2O_2, the colorless solution turned to brown immediately (Figure 2b). Upon the addition of 1 μL of 1 mg mL^{-1} MnME suspension to 100 μL of the mixture of DAB and H_2O_2, the colorless solution turned to brownish-black immediately (Figure 2c), indicating that MnME possessed the peroxidase-like activity to catalyze the oxidation of DAB in the presence of H_2O_2.

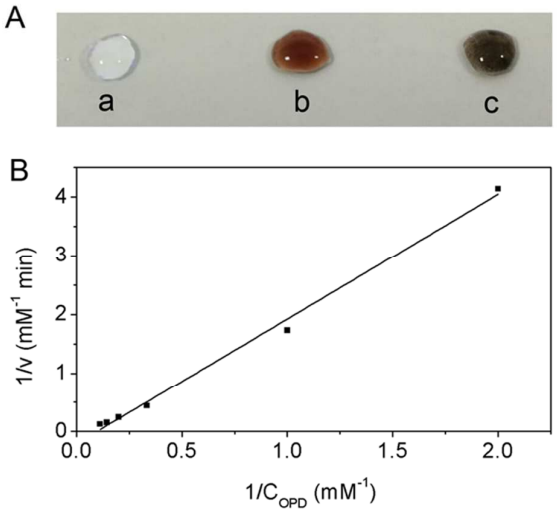

Figure 2. (A) Digital photo of mixtures: (a) DAB + H_2O_2, (b) HRP + DAB + H_2O_2, and (c) MnME + DAB + H_2O_2. The 1 mM H_2O_2, 0.4 mM DAB, and 1 mg·mL^{-1} MnME were used in the experiments. (B) Steady-state kinetic assay of OPD oxidation by MnME in 0.1 M HAc-NaAc (pH = 5.0) buffer. The H_2O_2 concentration was 10 mM.

The peroxidase-like catalytic activity of MnME was evaluated using an oxidation reaction of OPD by H_2O_2. The catalytic reaction was carried out with MnME at 10 mM H_2O_2 and 0.5, 1, 3, 5, 7 and 9 mM OPD, respectively. The reaction progress was monitored using UV−vis spectroscopy at 445 nm to measure the reaction rate. The reaction process followed the Michiaelis−Menten equation of $V = V_{max}[S]/(K_m + [S])$, where V_{max} is the maximum initial velocity, and [S] is the OPD concentration, and K_m is the Michaelis−Menten constant corresponding to the concentration at half-maximal velocity. The K_m of MnME in OPD oxidation reaction were calculated to be 0.50 mM, much lower than that of the natural HRP enzyme (0.81 mM),[43] indicating the higher affinity of the substrate to MnME. The catalytic constant (k_{cat}) of MnME is 236 min^{-1}, which is at least seven times higher than manganese-based mimicking enzymes including MnO_2 (163.68 min^{-1}),[44] MnTMPyP-dsDNA (56.8 min^{-1}),[45] indicating the higher catalytic activity.

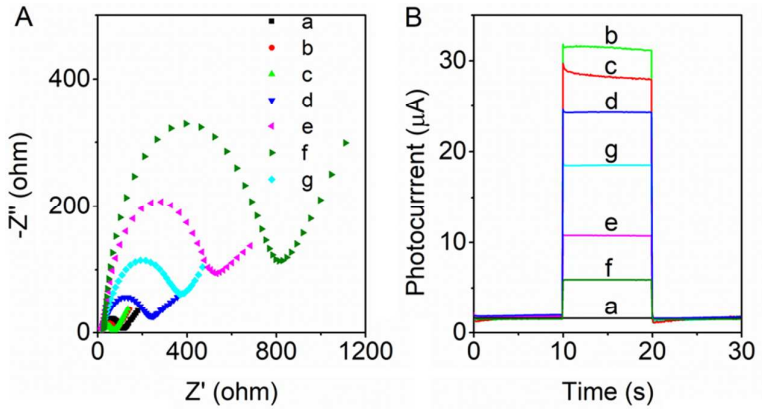

Figure 3. (A) Nyquist plots of EIS and (B) corresponding photocurrent responses of the modified ITO electrode: (a) ITO, (b) Bi_2S_3/ITO, (c) AuNPs/Bi_2S_3/ITO, (d) MCH/P1/AuNPs/Bi_2S_3/ITO, (e) MnME@AuNPs-P2/MCH/P1/AuNPs/Bi_2S_3/ITO, (f) MnME@AuNPs-P2/MCH/P1/AuNPs/Bi_2S_3/ITO after incubation with 1.0 mg mL^{-1} DAB and 0.01 M H_2O_2 for 5 min, (g) MnME@AuNPs-P2/MCH/P1/AuNPs/Bi_2S_3/ITO after reaction with 0.1 U μL^{-1} lambda exonuclease, 1 mM ATP and 1 U mL^{-1} T4 PNK, followed by incubation with DAB and H_2O_2.

Assay Feasibility. The preparation of photoelectrochemical biosensor was characterized by EIS and PEC. The electron-transfer resistance (R_{et}) was measured by the semicircle diameter of Nyquist plot (Figure 3A). A small semicircle diameter was observed in the bare ITO electrode as a result of the $[Fe(CN)_6]^{3-/4-}$ diffusion (Figure 3A, curve a). Moreover, a smaller R_{et} was detected in the Bi_2S_3-modified ITO electrode due to the high electronic conductivity of Bi_2S_3. The R_{et} value decreased when AuNPs were modified on the Bi_2S_3/ITO electrode (Figure 3A, curve c) due to the good conductivity of AuNPs, which facilitated the electron transfer from solution to the electrode. After assembling P1 and MCH on the AuNPs/Bi_2S_3/ITO electrode, a remarkable enhanced R_{et} value was obtained (Figure 3A, curve d). The increase in R_{et} may be ascribed to the immobilization of the negatively charged phosphoric acid backbone of P1 on the modified ITO electrode, which repelled the negatively charged $Fe(CN)_6^{3-/4-}$ and inhibited the electron transfer. Besides, the short alkanethiol of MCH blocked electron transfer from solution to the ITO electrode. Moreover, the R_{et} increased when MnME@AuNPs-P2 was assembled on the MCH/P1/AuNPs/Bi_2S_3/ITO electrode (Figure 3A, curve e). This increase can be explained by the steric hindrance of MnME@AuNPs and the electrostatic repulsion between the negatively charged phosphoric acid backbone of P2 and the negatively charged $Fe(CN)_6^{3-/4-}$.

After the incubation of the MnME@AuNPs-P2/MCH/P1/AuNPs/Bi_2S_3/ITO with 1.0 mg mL^{-1} DAB and 0.01 M H_2O_2 for 5 min, the R_{et} increased dramatically due to the MnME catalytic oxidation of DAB by H_2O_2, generating the insoluble and insulating product which can hinder the diffusion and electron transfer of $Fe(CN)_6^{3-/4-}$ to the electrode surface (Figure 3A, curve f). With the further addition of PNK, a significant decrease of R_{et} was observed (Figure 3A, curve g) due to the dissociation of the MnME@AuNPs-P2 conjugates from the surface of the AuNPs/Bi_2S_3/ITO electrode induced by the digestion of the phosphorylated dsDNA by lambda exonuclease, suggesting the success fabrication of the PEC biosensor.

To investigate the fabrication process of PEC sensor, we measured the photocurrent response of different photoelectrodes (Figure 3B). No photocurrent signal was measured in the bare ITO electrode (Figure 3B, curve a). After the assembly of Bi_2S_3 nanorods on the ITO electrode, a remarkable photocurrent of 31 μA was observed, indicating that Bi_2S_3 possessed good photoelectrical property (Figure 3B, curve b). After immobilization of AuNPs on the Bi_2S_3/ITO, the photocurrent decreased to 25 μA (Figure 3B, curve c) because the negatively charged AuNPs repelled the negative charged AA to the electrode surface. When P1 was self-assembled on the electrode surface via Au-S bond and subsequently blocked by MCH, the photocurrent decreased to 21 μA (Figure 3B, curve d). When the MnME@AuNPs-P2 conjugates were immobilized on the above modified electrode, the photocurrent further decreased to 10.8 μA (Figure 3B, curve e), demonstrating the successful deposition of the MnME@AuNPs-P2 conjugates on the electrode surface. The decrease of photocurrent may be explained by two factors: (1) the steric-hindrance effect of the modified MnME@AuNPs-P2 conjugates (it blocked the diffusion of electron donor of AA to electrode, resulting in an increased recombination rate of electron-hole pair of Bi_2S_3),[18] and (2) the electrostatic repulsion effect between the negative charged P1, P2 and the negative charged AA. When the MnME@AuNPs-P2/MCH/P1/AuNPs/Bi_2S_3/ITO incubated with DAB and H_2O_2, the photocurrent decreased significantly to 4.2 μA (Figure 3B, curve f) as a result of the MnME catalytic precipitation on the transducer surface. The MnME catalytic precipitation may hinder the diffusion and electron transfer of AA on the electrode/solution interface to the donate electron for the photogenerated holes of Bi_2S_3. In contrast, the presence of PNK may induce the digestion of the phosphorylated dsDNA by lambda exonuclease and the dissociation of the MnME@AuNPs-P2 conjugates from the surface of the AuNPs/Bi_2S_3/ITO electrode, resulting in the increase of photocurrent to 18.6 μA (Figure 3B, curve g). These results suggest the feasibility

of this PEC biosensor for PNK assay. In addition, the step-by-step assembly of AuNPs and MnME@AuNPs on the electrode surface was verified by AFM (Figure S2, see Supporting Information).

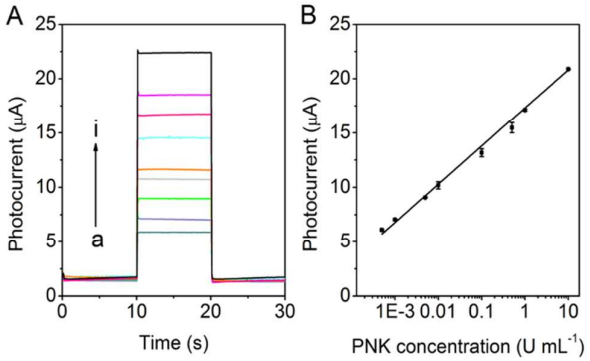

Figure 4. (A) Photocurrent responses of PEC biosensor in response to different-concentration T4 PNK (from a to i: 0, 0.0005, 0.001, 0.005, 0.01, 0.1, 0.5, 1, 10 U mL^{-1}). (B) The linear relationship between the photocurrent and the logarithm of PNK concentration. The 1.0 mM ATP and 0.1 U μL^{-1} lambda exonuclease were used in the experiments. The error bars show the standard deviation of 3 independent experiments.

Detection Sensitivity. Under the optimally experimental conditions (Figure S3, see Supporting Information), we monitored the variance of photocurrent in response to different-concentration PNK. As shown in Figure 4A, the photocurrent signal enhanced with the increasing PNK concentration, and the photocurrent exhibits a linear correlation with the logarithm of PNK concentration from 0.0005 to 10 U mL^{-1} (Figure 4B). The correlation equation was $I = 3.508 \log_{10} C + 17.31$ ($R^2 = 0.9988$), where I was photocurrent of PEC biosensor in response to PNK and C was the PNK concentration. The detection of limit (LOD) was estimated to be 1.27×10^{-5} U mL^{-1} by calculating the average control signal plus 3 times standard deviation. This method exhibited ultrahigh sensitivity, with 61-fold higher than that of the AuNP-based electrochemical biosensor (7.762×10^{-4} U mL^{-1}),[38] 79-fold higher than that of the DNAzyme-based signal-off PEC biosensor (1.0 mU mL^{-1}),[39] 79-fold higher than that of lambda exonuclease-based fluorescent biosensor,[46] 142-fold higher than that of amplification-involved electrochemical biosensor (0.0018 U mL^{-1}),[47] and 150-fold higher than that of rolling circle amplification-involved colorimetric biosensor (0.0019 U mL^{-1}).[48] The improved sensitivity of this PEC biosensor can be attributed to (1) the specific PNK-mediated phosphorylation, (2) the high lambda exonuclease-mediated cleavage efficiency towards the phosphorylated dsDNA, (3) the use of Bi_2S_3 nanorods

as the photoelectric conversion materials with low band gap; (4) the low background signal resulting from both the steric hindrance effect and catalytic precipitation effect of MnME@AuNPs.

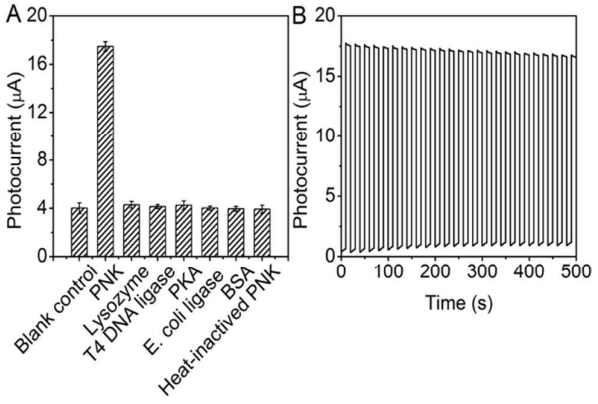

Figure 5. (A) The high specificity of the PEC biosensor towards PNK. The 1 U mL^{-1} PNK, 1 U mL^{-1} heat-inactivated T4 PNK, 10 μM BSA, 10 μM Lysozyme, 100 U mL^{-1} E. coli ligase, 100 U mL^{-1} T4 DNA ligase and 100 U mL^{-1} PKA were used in the experiments. Error bars show the standard deviation of 3 independent experiments. (B) Measurement of photocurrent after treatment by 1 U mL^{-1} PNK with light on and off.

Specificity and Stability of the PEC Biosensor. We used BSA, E. coli ligase, T4 DNA ligase, lysozyme, PKA, and the heat-inactivated T4 PNK as the interferences to investigate the specificity of the PEC biosensor. The T4 DNA ligase can catalyze the formation of a phosphodiester bond between the juxtaposed 5'-phosphate and the 3'-hydroxyl termini in duplex DNA or RNA; the PKA may facilitate the transfer of one or more gama-phosphate from ATP to specific amino acids (i.e., serine, threonine, and tyrosine residues) in target proteins; the E. coli ligase can catalyze the formation of a phosphodiester bond between the 5'-phosphate and the 3'-hydroxyl of two adjacent DNA strands in duplex DNA with cohesive ends. All these interferences do not have the catalysis function of PNK, and thus the dsDNA will not be cleaved by lambda exonuclease due to the lack of phosphorylation of DNA, resulting in the maintenance of the MnME@AuNPs-P2 conjugates on the surface of the P1/AuNPs/Bi_2S_3/ITO electrode. As a result, the photocurrent remained unchanged in the presence of these interferences (Figure 5A). In contrast, the presence of PNK may induce the digestion of the phosphorylated dsDNA by lambda exonuclease and the dissociation of the MnME@AuNPs-P2 conjugates

from the surface of the AuNPs/Bi_2S_3/ITO electrode and consequently the generation of an enhanced photocurrent (Figure 5A), suggesting that the PEC biosensor possesses high specificity towards T4 PNK.

The stability of biosensor was further investigated (Figure 5B). No significant change in photocurrent was observed with light on and off for more than 25 times with the interval of 10 s, indicating the good stability of biosensor. The reproducibility of biosensor was evaluated by intra- and inter-assay relative standard deviation (RSD). The intra-assay with a RSD of 6.27% was obtained by measuring 1 U mL^{-1} PNK for 10 times under the same conditions. The inter-assay precision with a RSD of 5.52% was obtained by measuring 1 U mL^{-1} PNK sample with five biosensors fabricated with the same process. These results demonstrated the good reproducibility of biosensor.

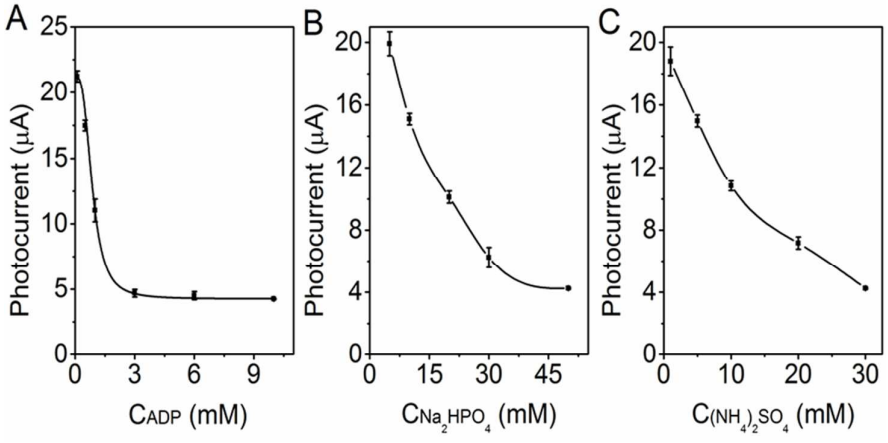

Figure 6. Measurement of photocurrent in the presence of ADP (A), Na_2HPO_4 (B) and $(NH_4)_2SO_4$ (C), respectively. The error bars show the standard deviation of 3 independent experiments.

PNK Inhibitor Assay. To investigate the capability of this PEC biosensor to screen the PNK inhibitors, we used $(NH_4)_2SO_4$, Na_2HPO_4 and ADP as the potential inhibitors, with no inhibition effect on the lambda exonuclease activity being found for them.[45] The ADP can induce a reversible phosphorylation reaction to severely inhibit the PNK activity.[49] As shown in Figure 6A, the photocurrent decreased in response to the increasing ADP concentration, and the half-maximal inhibition concentration (IC_{50}) of ADP was measured to be 1.23 mM, in agreement with that obtained by the nanochannel-based electrochemical assay (1 mM).[50] The Na_2HPO_4 and $(NH_4)_2SO_4$ can effectively inhibit the PNK activity through the salt effect.[51] As shown in

Figures 6B-C, the photocurrent decreased in response to the increasing Na_2HPO_4 (Figure 6B) and $(NH_4)_2SO_4$ concentration (Figure 6C), respectively. The IC_{50} value was measured to be 20.5 mM for Na_2HPO_4 and 16 mM for $(NH_4)_2SO_4$, in agreement with those obtained by the graphene oxide-based fluorescent assay (20 mM for Na_2HPO_4),[52] and the AuNP-mediated electrochemical assay (15 mM for $(NH_4)_2SO_4$).[38] In addition, we investigated the inhibition effects of 1 mM ADP, 20 mM Na_2HPO_4 and 10 mM $(NH_4)_2SO_4$ upon the PNK activity in HEK293T cells (Figure S4, see Supporting Information). These results indicate that this PEC biosensor has the capability to screen the PNK inhibitors.

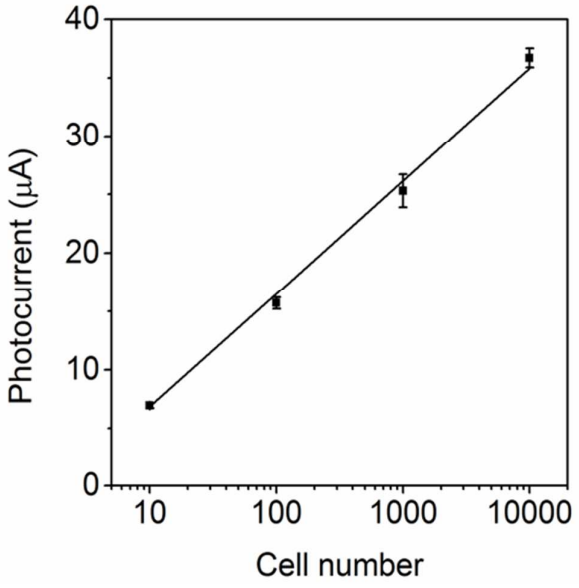

Figure 7. The linear correlation between the photocurrent and the logarithm of HEK-293 cell number from 5 to 10000 cells. Error bars show the standard deviations of 3 independent experiments.

Real Sample Analysis. To investigate the feasibility of this PEC biosensor for real sample analysis, we measured the PNK activity in HEK293T cells. Figure 7 shows the increase of photocurrent as a function of HEK293T cell number. In the logarithm scale, the photocurrent exhibited a linear correlation with the number of HEK293T cells in the range from 5 to 10000 cells, and the corresponding equation was $I = 8.786 \log_{10}X - 0.179$ ($R^2 = 0.995$), where X was the number of HEK-293 cells and I was the photocurrent, respectively. The limit of detection was estimated to be 2 cells by calculating the control group plus three times standard deviation. These results demonstrate that the great potentiality of the proposed method for practical

applications in clinical diagnosis and biomedical research.

CONCLUSION

In summary, we have developed for the first time a mimic peroxidase- and Bi_2S_3 nanorod-based PEC biosensor for signal-on detection of PNK on the basis of manganese-based mimic enzyme (MnME) catalytic precipitation. The mimic enzyme MnME has distinct advantages of easy synthesis and functionalized with biomolecules, higher catalytic activity than the manganese-based mimic enzyme. In the absence of PNK, MnME may stimulate the mimic enzyme catalytic precipitation onto the electrode surface, blocking the interfacial electron transfer due to the formation of an insulating barrier and the increase of steric hindrance and eventually leading to a low photocurrent. In contrast, the presence of PNK may induce the cleavage of the phosphorylated dsDNA by lambda exonuclease and the dissociation of the MnME@AuNPs conjugates from the electrode, leading to the decrease of catalytic precipitation on the surface of electrode and consequently the increase of interfacial electron transfer and the generation of a high photocurrent. This signal-on PEC biosensor exhibits high sensitivity with a detection limit of 1.27×10^{-5} U mL^{-1} and an extremely large dynamic range from 0.0005 to 10 U mL^{-1}. In addition, this PEC biosensor exhibits excellent specificity, high precision and good reproducibility. It can be further used to screen the potential PNK inhibitors and accurately quantify the PNK activity in cancer cells, holding great promise in clinic diagnosis and drug discovery.

ASSOCIATED CONTENT

Supporting Information

Scheme S1, Figures S1-S4 and the optimization of experimental conditions. This material is available free of charge via the Internet at http://pubs.acs.org.

AUTHOR INFORMATION

Corresponding Author

*Tel.: +86 0531-86186033. Fax: +86 0531-82615258. E-mail: cyzhang@sdnu.edu.cn.

Author Contributions

†These authors contributed equally.

Notes

The authors declare no competing financial interest.

ACKNOWLEDGMENTS

This work was supported by the National Natural Science Foundation of China (Grant Nos. 21325523, 21527811, 21735003 and 21605096), and the Award for Team Leader Program of Taishan Scholars of Shandong Province, China.

REFERENCES

(1) Zhao, W. W.; Xu, J. J.; Chen, H. Y. Photoelectrochemical bioanalysis: the state of the art. *Chem. Soc. Rev.* **2015**, *44*, 729-741.

(2) Zhao, W. W.; Xu, J. J.; Chen, H. Y. Photoelectrochemical DNA biosensors. *Chem. Rev.* **2014**, *114*, 7421-7441.

(3) Tu, W.; Cao, H.; Zhang, L.; Bao, J.; Liu, X.; Dai, Z. H. Dual signal amplification using gold nanoparticles-enhanced zinc selenide nanoflakes and P19 protein for ultrasensitive photoelectrochemical biosensing of MicroRNA in cell. *Anal. Chem.* **2016**, *88*, 10459-10465.

(4) Tanne, J.; Schafer, D.; Khalid, W.; Parak, W. J.; Lisdat, F. Light-controlled bioelectrochemical sensor based on CdSe/ZnS quantum dots. *Anal. Chem.* **2011**, *83*, 7778-7785.

(5) Chen, D.; Zhang, H.; Li, X.; Li, J. Biofunctional titania nanotubes for visible-light-activated photoelectrochemical biosensing. *Anal. Chem.* **2010**, *82*, 2253-2261.

(6) Li, H.; Li, J.; Xu, Q.; Hu, X. Poly(3-hexylthiophene)/TiO_2 nanoparticle-functionalized electrodes for visible light and low potential photoelectrochemical sensing of organophosphorus pesticide chlopyrifos. *Anal. Chem.* **2011**, *83*, 9681-9686.

(7) Tran, F.; Blaha, P. Accurate band gaps of semiconductors and insulators with a semilocal exchange-correlation potential. *Phys. Rev. Lett.* **2009**, *102*, 226401.

(8) Wang, H.; Zhang, Q.; Yin, H.; Wang, M.; Jiang, W.; Ai, S. Photoelectrochemical immunosensor for methylated RNA detection based on G-C_3N_4/CdS quantum dots heterojunction and phos-tag-biotin. *Biosens. Bioelectron.* **2017**, *95*, 124-130.

(9) Yan, K.; Wang, R.; Zhang, J. A Photoelectrochemical biosensor for o-aminophenol based on assembling of CdSe and DNA on TiO_2 film electrode. *Biosens. Bioelectron.* **2014**, *53*, 301-304.

(10) Li, X.; Zhu, L.; Zhou, Y.; Yin, H.; Ai, S. Enhanced photoelectrochemical method for sensitive detection of protein kinase a activity using TiO_2/gC_3N_4, PAMAM dendrimer, and alkaline phosphatase. *Anal. Chem.* **2017**, *89*, 2369-2376.

(11) Guangfeng, W.; Ling, C.; Xiuping, H.; Yanhong, Z.; Xiaojun, Z. Detection of polynucleotide kinase activity by using a gold electrode modified with magnetic microspheres coated with titanium dioxide nanoparticles and a DNA dendrimer. *Analyst* **2014**, *139*, 3895-3900.

(12) Wang, G. L.; Shu, J. X.; Dong, Y. M.; Wu, X. M.; Zhao, W. W.; Xu, J. J.; Chen, H. Y. Using G-quadruplex/hemin to "switch-on" the cathodic photocurrent of p-type PbS quantum dots: toward a versatile platform for photoelectrochemical aptasensing. *Anal. Chem.* **2015**, *87*, 2892-2900.

(13) Tahir, A. A.; Ehsan, M. A.; Mazhar, M.; Wijayantha, K. G. U.; Zeller, M.; Hunter, A. D. Photoelectrochemical and photoresponsive properties of Bi_2S_3 nanotube and nanoparticle thin films. *Chem. Mater.* **2010**, *22*, 5084-5092.

(14) Yin, H.; Sun, B.; Zhou, Y.; Wang, M.; Xu, Z.; Fu, Z.; Ai, S. A New strategy for methylated DNA detection based on photoelectrochemical immunosensor using Bi_2S_3 nanorods, methyl bonding domain protein and anti-his tag antibody. *Biosens. Bioelectron.* **2014**, *51*, 103-108.

(15) Zhou, Y.; Xu, Z.; Wang, M.; Sun, B.; Yin, H.; Ai, S. DNA methyltransferase activity assay based on visible light-activated photoelectrochemical biosensor. *Biosens. Bioelectron.* **2014**, *53*, 263-267.

(16) Huang, W.; Xing, C.; Wang, Y.; Li, Z.; Wu, L.; Ma, D.; Dai, X.; Xiang, Y.; Li, J.; Fan, D.; Zhang, H. Facile fabrication and characterization of two-dimensional bismuth (III) sulfide nanosheets for high-performance photodetector applications under ambient conditions. *Nanoscale* **2018**, *10*, 2404-2412.

(17) Ye, C.; Wang, M. Q.; Gao, Z. F.; Zhang, Y.; Lei, J. L.; Luo, H. Q.; Li, N. B. Ligating dopamine as signal trigger onto the substrate via metal-catalyst-free click chemistry for "signal-on" photoelectrochemical sensing

of ultralow microRNA levels. *Anal. Chem.* **2016**, *88*, 11444-11449.

(18) Sun, B.; Qiao, F.; Chen, L.; Zhao, Z.; Yin, H.; Ai, S. Effective signal-on photoelectrochemical immunoassay of subgroup J avian leukosis virus based on Bi_2S_3 nanorods as photosensitizer and in situ generated ascorbic acid for electron donating. *Biosens. Bioelectron.* **2014**, *54*, 237-243.

(19) Okoth, O. K.; Yan, K.; Liu, Y.; Zhang, J. Graphene-doped Bi_2S_3 nanorods as visible-light photoelectrochemical aptasensing platform for sulfadimethoxine detection. *Biosens. Bioelectron.* **2016**, *86*, 636-642.

(20) Zhao, W. W.; Ma, Z. Y.; Yan, D. Y.; Xu, J. J.; Chen, H. Y. In situ enzymatic ascorbic acid production as electron donor for CdS quantum dots equipped TiO_2 nanotubes: a general and efficient approach for new photoelectrochemical immunoassay. *Anal. Chem.* **2012**, *84*, 10518-10521.

(21) Zhu, Y. C.; Zhang, N.; Ruan, Y. F.; Zhao, W. W.; Xu, J. J.; Chen, H. Y. Alkaline phosphatase tagged antibodies on gold nanoparticles/TiO_2 nanotubes electrode: a plasmonic strategy for label-free and amplified photoelectrochemical immunoassay. *Anal. Chem.* **2016**, *88*, 5626-5630.

(22) Wang, G. L.; Yuan, F.; Gu, T.; Dong, Y.; Wang, Q.; Zhao, W. W. Enzyme-initiated quinone-chitosan conjugation chemistry: toward a general in situ strategy for high-throughput photoelectrochemical enzymatic bioanalysis. *Anal. Chem.* **2018**, *90*, 1492-1497.

(23) Zhao, W.-W.; Yu, P.-P.; Xu, J.-J.; Chen, H.-Y. Ultrasensitive photoelectrochemical biosensing based on biocatalytic deposition. *Electrochem. Commun.* **2011**, *13*, 495-497.

(24) Zhang, X.; Liu, M.; Mao, Y.; Xu, Y.; Niu, S. Ultrasensitive photoelectrochemical immunoassay of antibody against tumor-associated carbohydrate antigen amplified by functionalized graphene derivates and enzymatic biocatalytic precipitation. *Biosens. Bioelectron.* **2014**, *59*, 21-27.

(25) Zhao, W. W.; Ma, Z. Y.; Yu, P. P.; Dong, X. Y.; Xu, J. J.; Chen, H. Y. Highly sensitive

photoelectrochemical immunoassay with enhanced amplification using horseradish peroxidase induced biocatalytic precipitation on a CdS quantum dots multilayer electrode. *Anal. Chem.* **2012**, *84*, 917-923.

(26) Xiao, Y.; Qu, X.; Plaxco, K. W.; Heeger, A. J. Label-free electrochemical detection of DNA in blood serum via target-induced resolution of an electrode-bound DNA pseudoknot. *J. Am. Chem. Soc.* **2007**, *129*, 11896-11897.

(27) Xiao, Y.; Piorek, B. D.; Plaxco, K. W.; Heeger, A. J. A reagentless signal-on architecture for electronic, aptamer-based sensors via target-induced strand displacement. *J. Am. Chem. Soc.* **2005**, *127*, 17990-17991.

(28) Wu, D.; Yin, B. C.; Ye, B. C. A Label-free electrochemical DNA sensor based on exonuclease III-aided target recycling strategy for sequence-specific detection of femtomolar DNA. *Biosens. Bioelectron.* **2011**, *28*, 232-238.

(29) Cui, L.; Yin, H.; Dong, J.; Fan, H.; Liu, T.; Ju, P.; Ai, S. A Mimic peroxidase biosensor based on calcined layered double hydroxide for detection of H_2O_2. *Biosens. Bioelectron.* **2011**, *26*, 3278-3283.

(30) Song, Y.; Qu, K.; Zhao, C.; Ren, J.; Qu, X. Graphene oxide: intrinsic peroxidase catalytic activity and its application to glucose detection. *Adv. Mater.* **2010**, *22*, 2206-2210.

(31) Ling, P.; Zhang, Q.; Cao, T.; Gao, F. Versatile three-dimensional Porous Cu@Cu_2O aerogel networks as electrocatalysts and mimicking peroxidases. *Angew. Chem. Int. Ed.* **2018**, *57*, 6819-6824.

(32) Mu, J.; Wang, Y.; Zhao, M.; Zhang, L. Intrinsic peroxidase-like activity and catalase-like activity of Co_3O_4 nanoparticles. *Chem. Commun.* **2012**, *48*, 2540-2542.

(33) Zang, Y.; Lei, J.; Zhang, L.; Ju, H. In situ generation of electron acceptor for photoelectrochemical biosensing via hemin-mediated catalytic reaction. *Anal. Chem.* **2014**, *86*, 12362-12368.

(34) Zang, Y.; Lei, J.; Ling, P.; Ju, H. Catalytic hairpin assembly-programmed porphyrin–DNA complex as photoelectrochemical initiator for DNA biosensing. *Anal. Chem.* **2015**, *87*, 5430-5436.

(35) Gong, L.; Dai, H.; Zhang, S.; Lin, Y. Silver iodide-chitosan nanotag induced biocatalytic precipitation for self-enhanced ultrasensitive photocathodic immunosensor. *Anal. Chem.* **2016**, *88*, 5775-5782.

(36) Wang, G. L.; Shu, J. X.; Dong, Y. M.; Wu, X. M.; Li, Z. J. An ultrasensitive and universal photoelectrochemical immunoassay based on enzyme mimetics enhanced signal amplification. *Biosens. Bioelectron.* **2015**, *66*, 283-289.

(37) Wang, H.; Zhu, L.; Duan, J.; Wang, M.; Yin, H.; Wang, P.; Ai, S. Photoelectrochemical biosensor for HEN1 RNA methyltransferase detection using peroxidase mimics PtCu NFs and poly (U) polymerase-mediated RNA extension. *Biosens. Bioelectron.* **2018**, *103*, 32-38.

(38) Cui, L.; Li, Y.; Lu, M.; Tang, B.; Zhang, C. Y. An ultrasensitive electrochemical biosensor for polynucleotide kinase assay based on gold nanoparticle-mediated lambda exonuclease cleavage-induced signal amplification. *Biosens. Bioelectron.* **2018**, *99*, 1-7.

(39) Zhuang, J.; Lai, W.; Xu, M.; Zhou, Q.; Tang, D. Plasmonic AuNP/g-C_3N_4 nanohybrid-based photoelectrochemical sensing platform for ultrasensitive monitoring of polynucleotide kinase activity accompanying DNAzyme-catalyzed precipitation amplification. *ACS Appl Mater Interfaces* **2015**, *7*, 8330-8338.

(40) Zhang, Y. Z.; Cheng, T.; Wang, Y.; Lai, W. Y.; Pang, H.; Huang, W. A Simple approach to boost capacitance: flexible supercapacitors based on manganese oxides@ MOFs via chemically induced in situ self-transformation. *Adv. Mater.* **2016**, *28*, 5242-5248.

(41) Ambrosi, A.; Castaneda, M. T.; Killard, A. J.; Smyth, M. R.; Alegret, S.; Merkoci, A. Double-codified gold nanolabels for enhanced immunoanalysis. *Anal. Chem.* **2007**, *79*, 5232-5240.

(42) Ge, Z.-H.; Zhang, B. P.; Yu, Z.-X.; Jiang, B. B. Controllable synthesis: Bi_2S_3 nanostructure powders and highly textured polycrystals. *CrystEngComm* **2012**, *14*, 2283-2288.

(43) Feng, D.; Gu, Z. Y.; Li, J. R.; Jiang, H. L.; Wei, Z.; Zhou, H. C.; Zhou, H. C. Zirconium□ metalloporphyrin PCN-222: mesoporous metal–organic frameworks with ultrahigh stability as biomimetic catalysts. *Angew. Chem.* **2012**, *51*, 10307-10310.

(44) Liu, X.; Wang, Q.; Zhao, H.; Zhang, L.; Su, Y.; Lv, Y. BSA-templated MnO_2 nanoparticles as both peroxidase and oxidase mimics. *Analyst* **2012**, *137*, 4552-4558.

(45) Xu, J.; Wu, J.; Zong, C.; Ju, H.; Yan, F. Manganese porphyrin-dsDNA complex: a mimicking enzyme for highly efficient bioanalysis. *Anal. Chem.* **2013**, *85*, 3374.

(46) Hou, T.; Wang, X.; Liu, X.; Lu, T.; Liu, S.; Li, F. Amplified detection of T4 polynucleotide kinase activity by the coupled λ exonuclease cleavage reaction and catalytic assembly of bimolecular beacons. *Anal. Chem.* **2014**, *86*, 884, 884-890.

(47) Zhang, Q.; Li, Z.; Zhou, Y.; Li, X.; Li, B.; Yin, H.; Ai, S. Electrochemical biosensors for polynucleotide kinase activity assay and inhibition screening based on phosphorylation reaction triggered λ exonuclease and exonuclease I cleavage. *Sens. Actuators B* **2016**, *225*, 151-157.

(48) Jiang, H. X.; Kong, D. M.; Shen, H. X. Amplified detection of DNA ligase and polynucleotide kinase/phosphatase on the basis of enrichment of catalytic G-quadruplex DNAzyme by rolling circle amplification. *Biosens. Bioelectron.* **2014**, *55*, 133-138.

(49) Tang, Z.; Wang, K.; Tan, W.; Ma, C.; Li, J.; Liu, L.; Guo, Q.; Meng, X. Real-time investigation of nucleic acids phosphorylation process using molecular beacons. *Nucleic Acids Res.* **2005**, *33*, e97.

(50) Lin, L.; Liu, Y.; Yan, J.; Wang, X.; Li, J. Sensitive nanochannel biosensor for T4 polynucleotide kinase activity and inhibition detection. *Anal. Chem.* **2013**, *85*, 334-340.

(51) Lillehaug, J. R.; Kleppe, K. Effect of salts and polyamines on T4 polynucleotide kinase. *Biochemistry* **1975**, *14*, 1225-1229.

(52) Lin, L.; Liu, Y.; Zhao, X.; Li, J. Sensitive and rapid screening of T4 polynucleotide kinase activity and inhibition based on coupled exonuclease reaction and graphene oxide platform. *Anal. Chem.* **2011**, *83*, 8396-8402.

For TOC only

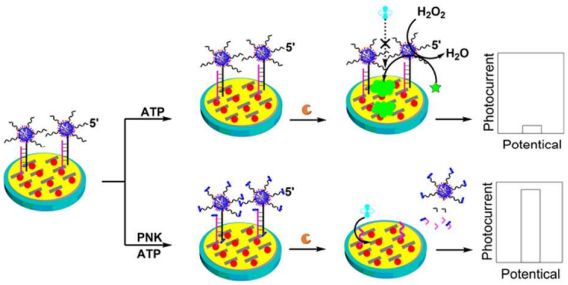
5'
ATP
PNK
ATP
5'
C
H_2O_2
H_2O
Photocurrent
Potentical
5'
C
Photocurrent
Potentical